Available online at www.sciencedirect.com
SCIENCE DIRECT®
Earth-Science Reviews 71 (2005) 127–146
EARTH-SCIENCE REVIEWS
www.elsevier.com/locate/earscirev

Microphysical and optical properties of noctilucent clouds

Alexander A. Kokhanovsky*

Institute of Environmental Physics, Bremen University, Otto Hahn Allee 1, D-28213 Bremen, Germany

Received 12 January 2004; accepted 21 February 2005

Abstract

Noctilucent clouds play an important role in the physics of the summer polar mesopause. They consist of tiny ice crystals with characteristic dimensions smaller than 200 nm. However, neither exact shape of particles nor their precise chemical composition or concentration is known with a high accuracy. Also the origin of the particulate layer at such a high level in the terrestrial atmosphere (about 80 km) is a matter of a considerable controversy.

This paper summarizes recent advances in our understanding of nature of noctilucent clouds (NLCs) with special emphasis on the size and shape of crystals.

Keywords: noctilucent clouds; light scattering; mesosphere; ice crystals

1. Introduction

The lowest temperatures in the terrestrial atmosphere are reached at the height range 80–90 km in areas surrounding the poles. For instance, they are close to 150 K (≈ −123 °C) in summer at these heights. Smaller values (e.g., 100–150 K and even below this limit) have also been reported (Schmidlin, 1991; Lübken and Müllemann, 2003). Such low values of temperature allow the formation of water molecular clusters and even macroscopic ice particles. These particles have typical characteristic sizes (e.g., radii of volume-equivalent spheres) in the range 50–100 nm and are of a nonspherical shape.

The presence of particles produces the enhanced light scattering in correspondent atmospheric layers (Gadsden and Schröder, 1989). This enhanced light scattering in the mesosphere has been observed from ground, satellite and rocket-borne measurements. It is believed that Leslie (1885) was first to report on the phenomenon in the scientific magazine, although similar observations were presented by Backhouse (1885) and Jesse (1886) about at the same time. In particular, Leslie (1885) wrote:

But I have seen nothing in the way of twilight effect so strange as that of Monday evening, the 6th, when about 10 p.m. a sea of luminous silvery white clouds lay above a belt of ordinary clear twilight sky, which

* Tel.: +49 421218 4475; fax: +49 421218 4555.
E-mail address: alexk@iup.physik.uni-bremen.de.

0012-8252/$ - see front matter © 2005 Elsevier B.V. All rights reserved.
doi:10.1016/j.earscirev.2005.02.005

was rather low in tone and colour. These clouds were wave-like in form, and evidently at a great elevation, and though they must have received their light from the sun, it was not easy to think so, as upon the dark sky they looked brighter and paler than clouds under a full moon.

A photo of such clouds, which are often called noctilucent clouds (NLCs), is given in Fig. 1. The description of Leslie can be well applied to this photo although it was taken at a different time and place. A wave-like structure in Fig. 1 is due to gravity waves (Thayer et al., 2003).

NLCs are very tenuous objects (typically, the optical thickness ~10^{-4} or even below this value). Therefore, they can be seen from the ground by scattering of solar light only during twilight, when the observer and the atmosphere below clouds are in darkness while the clouds themselves remain sunlit. This condition occurs for solar depression angles 6–16° (Avaste et al., 1980; Taylor et al., 2002). Von Zahn and Berger (2003) argue that in midsummer a persistent cloud of icy particles covers the summer pole down to about 60° latitude at mesopause heights. Particles are too small, however, to cause visible NLCs.

It comes as a great surprise that apparently NLCs have not been noted till 1885 (Gadsden and Schröder, 1989). It allows for a hypotheses that their properties have been changed in industrial era in such extent that they become visible (e.g., due to larger sizes of particles). If this assumption is indeed true, then NLCs give early warning to us in respect to global climate changes (e.g., see Klostermeyer, 2002; Shettle et al., 2002). This assumption, however, remains to be proved. In particular, disastrous eruptions occurred on Krakatoa, an island near the coast of Java in 1883. At the same year Leslie (1885) noted an abnormal glare both before and after sunset. So it is of importance to study the influence of volcanic activity on NLCs.

The task of this paper is to present the modern knowledge on NLC microphysical and optical characteristics in a short and concise form. Note that first 100 years of NLC studies have been reviewed by Gadsden and Schröder (1989). So we concentrate mostly on results obtained in recent years, although the main findings from a previous research (see, e.g., reviews by Willmann et al., 1973; Vasilyev and Rodionov, 1975; Avaste et al., 1980) are also given.

2. The size of crystals

Noctilucent clouds formation is governed by the degree of saturation $S=P_{H_2O}/P_S$, where P_{H_2O} is the partial pressure of water vapor and P_S is the saturation pressure of water vapor over ice. Crystals in NLCs can exist and grow if $S>1$, i.e. $P_S<P_{H_2O}$. The value of P_S depends on temperature. In particular, Martie and Mauersberger (1993) give the following relationship: $\lg P_S=c_1-c_2/T$, where $\lg\equiv\log_{10}$, $c_1=2.537$, $c_2=2663.5$, P_S is in N/m^{2}and T is in K. The frost point temperature T_f is defined as such a temperature for which it holds: $P_S=P_{H_2O}$. Then it follows: $T_f=c_2(c_1-\lg P_{H_2O})^{-1}$. Clearly, P_{H_2O} varies with the height h (see, e.g., Körner and Sonnemann, 2001). The substitution of the function $P_{H_2O}(h)$ in equation given above allows us to find $T_f(h)$.

Fig. 1. Typical pattern of NLCs (courtesy of T. Eklund).

The height dependence of the frost point temperature is given in Fig. 2 for two assumptions on water vapor concentration profiles (Lübken and Müllemann, 2003). The long-dashed line (see cross in Fig. 2) shows $T_f(h)$ using a water vapor mixing ratio of 5 ppmv independent of altitude. The short-dashed line accounts for the model of the water vapor given by Körner and Sonnemann (2001). Both assumptions produce very similar results. Solid lines in Fig. 2 show the results of measurements performed on July 16th and September 14th, 2001(Lübken and Müllemann, 2003). We see that the value of T_f is not reached on September 14th, 2001 (so no NLCs can appear). However, starting from the cross in Fig. 2 (around 80 km) and up to 90 km the measured temperature (on July 16th, 2001) is smaller than T_f. This allows for the formation of NLCs. Note that dashed-dotted lines in Fig. 2 show the corresponding mean profiles given by

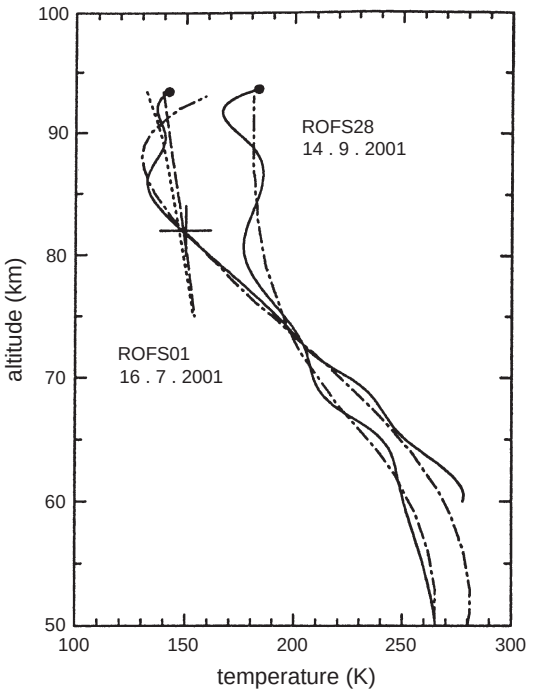

Fig. 2. The dependence of the frost temperature on the height (the short-dashed line). The long-dashed line shows T_f using a water vapor mixing ratio of 5 ppmv independent of altitude. Temperature profiles obtained from measurements (solid lines) also are given. The dashed-dotted lines show the corresponding mean profiles from 69°N from the study of Lübken et al. (1999). This figure is taken from study of Lübken and Müllemann (2003) (their fig. 1).

Table 1
Average properties of NLCs (Avaste et al., 1980)

Color	Bluish white
Height	82.7 km
Latitude of ground observations	45–80°, best visible at about 60°
Season of ground observations in northern hemisphere	March–October, best in June–August
Time of observation	Nautical and part of astronomical twilight, while the solar depression angle varies from 6° to 16°
Spatial extent	10,000–4,000,000 km^2
Duration	Several minutes to more than 5 h
Average velocity	40 m/s towards SW; individual bands often move in different directions and at a speed different from the speed of the display as a whole
Thickness	0.5–2 km
Vertical wave amplitude	1.5–3.0 km
Temperature in the presence of NLCs	135 K
Number density of particles	0.01–1 cm^{-3}
Average radius	150 nm

Lübken et al. (1999) for 69°N. Usually NLCs are observed somewhat below the minimal temperature level. This is best explained by the descent of particles to lower layers as they grow. In particular, Avaste et al. (1980) state that the average NLC height is 82.7 km. This is somewhat below the minimum of temperature given in Fig. 2. Avaste et al. (1980) also compiled the list of other important characteristics of NLCs. They are given in Table 1. In addition to Table 1, we add that the typical cloud optical thickness is 10^{-4}. This means that the extinction coefficient σ_{ext} for 1-km-thick cloud is around 10^{-4} km^{-1}. McHugh et al. (2003) report values of 10^{-7}–10^{-4} cm $^{-1}$ in the spectral range 2.45–6.26 μm as derived from the Halogen Occultation Experiment (HALOE).

It should be pointed out, however, that supersaturation is not always required for the NLC existence (Stevens et al., 2001). So more studies are needed.

Fig. 2 indirectly confirms that water ice is the primary component of NLCs. Another indirect confirmation is offered by Hervig et al. (2001), who derived NLC extinction coefficients from HALOE. Eight HALOE channels in the spectral

range 2.45–10 μm show remarkable agreement with model spectra based on ice particle extinction with effective radii between 69 an 128 nm. A call for a similar experiment was given by Witt (1969). He proposed to investigate the scattering properties of NLCs in spectral regions where ice possesses absorption bands (e.g., at 3240 cm^{-1}). Then NLC particles are certainly Rayleigh scatterers and effects of their shapes are considerably reduced (Bohren, 1983). This simplifies the interpretation.

Note that an ice particle model was not favoured by early works (see, e.g., Ludlam (1957)). Ludlam (1957) underlined that it is of importance to understand upon what nuclei NLC particles form. He found that the deduced concentrations of NLC particles suggest a nucleated rather than a homogeneous nucleation. The problem of NLC nuclei, therefore, requires a considerable attention. Note, that the possibility of ionic nucleation was discussed by Gumbel et al. (2003), who largely discarded this growth mechanism. Yet another possibility is the flux of extraterrestrial particles (Hunten et al., 1980). It is unlikely that terrestrial particles propagate to the mesosphere and serve as nuclei there. In particular, last volcanic eruptions (e.g., Mt. Pinatubo) did not alter observable properties of NLCs.

The information on the size of ice crystals in NLCs is poor. In particular, it cannot be compared to the level of detail we have with respect to tropospheric clouds (Kokhanovsky, 2004). This is mostly due to the fact that NLCs occur at heights where the collection of particles becomes a problem. Another difficulty arises due to the fact that some particles trapped by specially designed rocket-borne collectors have been from outside of NLCs (e.g., in lower atmosphere). This makes an interpretation of measurements even harder.

Attempts for direct sampling of crystals in NLCs are reported by Hemenway and Witt (1963), Hemenway et al. (1964), Farlow (1968), Farlow and Ferry (1972), Farlow et al. (1970), Rauser and Fechtig (1972) among others. Farlow et al. (1970) and Farlow and Ferry (1972) reported that their collectors were able to detect NLC particles with effective radii a in the range 25–200 nm. Farlow and Ferry (1972) found that the maximum of the particle size distribution in the NLC event they observed was located around 73 nm (see Fig. 3). Generally, the particle size distribution is characterized by a rapid increase for small particles and more slow decrease from the maximum in the larger particles range (Gadsden and Schröder, 1989). This is a characteristic feature of particles in tropospheric clouds as well (Kokhanovsky, 2004).

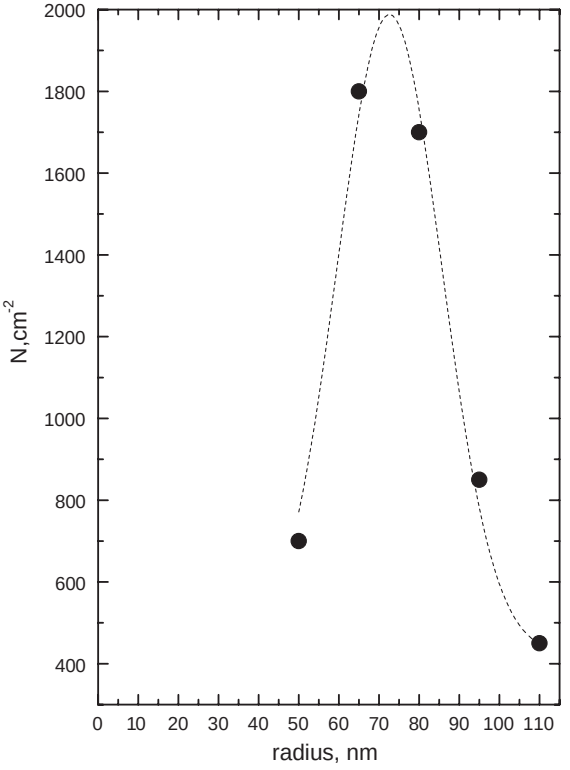

Fig. 3. The dependence of the concentration of particles on the unit area of a collecting surface (Farlow and Ferry, 1972).

Comprehensive data sets on the size on NLC particles have been accumulated using interpretation of spectral slopes of the scattered light intensity and the degree of polarization of scattered light (Gadsden and Schröder, 1989). Retrievals of sizes from optical data were done using Mie theory (see Appendix A), which is valid for spherical scatterers only. This may bias results (Mishchenko, 1991). Another problem is due to the fact that the refractive index m of NLC crystals, which serves as input to the Mie theory calculations, is poorly known. It is usually assumed that it coincides with that of ice (see Fig. 4). However, the value of the ice refractive index $m=n-i\kappa$ depends on the temperature T and ice structure. Crystals formed at temperatures below 120 K will

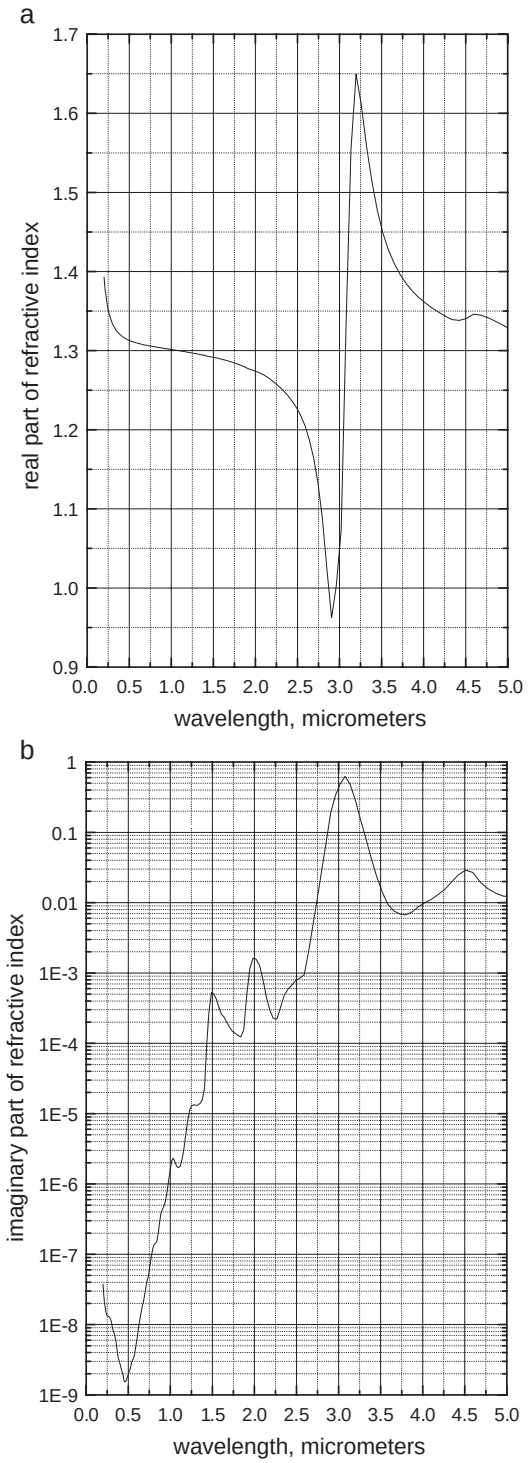

Fig. 4. The real (a) and imaginary (b) parts of the refractive index of ice (Warren, 1984).

be amorphous; cubic ice forms between 120 K and 150 K; hexagonal ice is the main structure above 150 K (Hobbs, 1974; Gadsden, 1977a; Mayer and Hallbrucker, 1987). Measurements of the refractive index of ice as the function of the wavelength λ at 120–150 K are rare.

Summing up, optical particle sizing in NLCs is routinely done using two major assumptions, namely that particles are spheres and the refractive index of particles corresponds to that of ice at −20 °C (see Fig. 4). Both assumptions are hardly valid. The error δ introduced by them is not clear at the moment. Note that δ decreases with the size parameter $x=2\pi a/\lambda$.

Other potential sources of errors are due to illumination of NLC particles not only by direct solar light but also by scattered light from regions outside NLCs (both from above and below, see Fig. 1). It is difficult to account for this effect in a correct way. The situation is even worse for ground-based measurements. Then the spectral attenuation on the long path from NLC to an observer should be fully accounted for, which is not an easy task taking into account the spectral atmospheric extinction variability.

The most reliable data come from rocket-borne polarimetry. In particular, Tozer and Beeson (1974) found that the linear polarization is in the range 0.94–0.96 at scattering angles 80–84°. Similar results were reported by Heintzenberg et al. (1978). This confirms extremely small dimensions of NLC particles.

We present selected results of polarization measurements by a rocket-borne instrument at wavelengths 490 and 610 nm in Fig. 5 (Witt, 1960). Theoretical results for molecular and particle scattering are also shown. One can see that the presence of monodispersed spheres having the radius 130 nm and the refractive index 1.31 is capable of explaining results of measurements. Experimental data of Tozer and Beeson (1974) are given in Fig. 5 by triangles and stars. Note that the Rayleigh-type polarization similar to that given in Fig. 5 can be produced by much larger nonspherical particles (Zakharova and Mishchenko, 2000). However, very large ice particles do not exist in mesosphere due to low concentration of water vapor there.

Clearly, there is no reason for NLC particles to be of the same size. Therefore, spherical polydispersed models have been used extensively for the interpretation of optical measurements. In particular, Heintzenberg et al. (1978) used the truncated lognormal

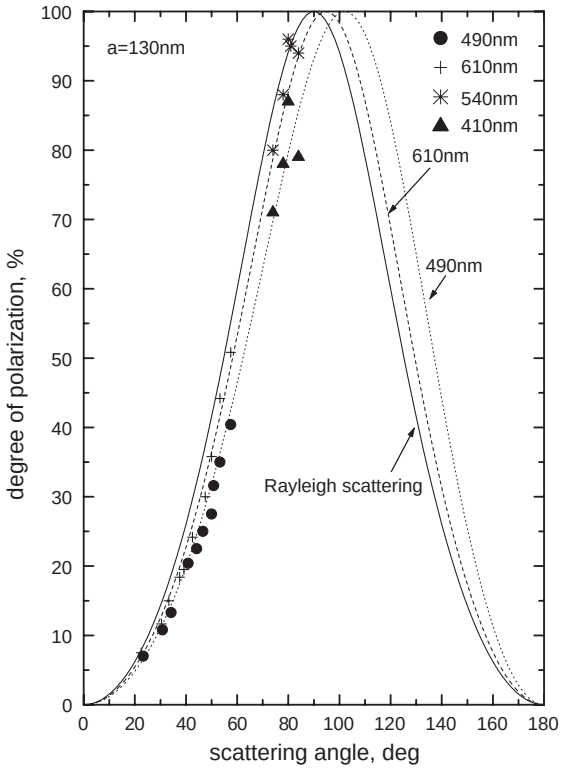

Fig. 5. The degree of polarization of solar light scattered by ice crystals in NLC measured by the rocket-borne instrument (Witt, 1960) at wavelengths 490 and 610 nm (symbols). Results of calculations for the spherical particles having the radius of 130 nm and the refractive index equal to 1.31 are shown by dashed lines. The solid line gives the angular dependence of polarization according to the Rayleigh law. Experimental results obtained by Tozer and Beeson (1974) are also given.

distribution for the interpretation of measured degree of linear polarization of scattered light in NLCs. Note that values close to 90% at 80° scattering angle have been found by Heintzenberg et al. (1978) at $\lambda = 214$, 366, 453, and 536 nm. This also points to small values of the crystal sizes in NLCs.

However, the problem of ambiguity arises for polydispersed models. Presumably, several different particle size distributions can be used for the interpretation of the same experimental data. So we prefer to use the monodispersed model in this paper. This also facilitates comparisons of data obtained from different sources.

A similar conclusion in respect to polydispersed models has been reached by Gumbel et al. (2001) and Gumbel and Witt (2001), who measured the

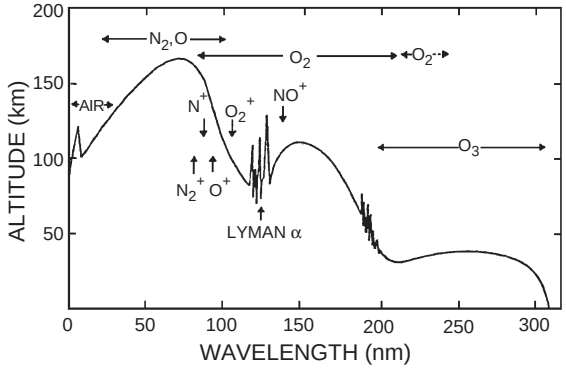

Fig. 6. Altitude (in km) to which solar radiation penetrates at different wavelengths. The spectral regions in which N_2, O, O_2, and O_3 absorb radiation are indicated. The ionization thresholds for several atmospheric constituents are also shown (Brasseur, 1996).

phase function $p(\theta)$ of a strong NLC event by a rocket-borne photometer at the wavelength 222 nm and scattering angles $\theta = 50$–$115°$. Then the illumination of a cloud studied from the lower atmosphere can be neglected due to ozone absorption at this wavelength (see Fig. 6). Experimental data are shown in Fig. 7 together with theoretical results for particles having the equivalent radius of a sphere a, which is equal to 30, 42, and 50 nm. We see that the monodispersed spheres with radii 42 nm are capable of explaining measured data. Then the number density N of particles can be retrieved from the measurements of the absolute radiance. The meas-

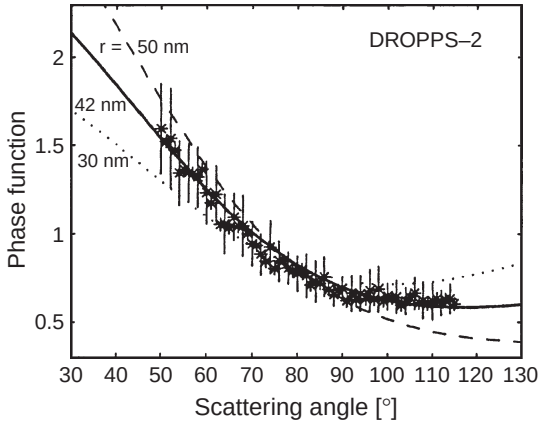

Fig. 7. The angular dependence of scattering at 220 nm. Error bars show the statistical scatter of detected radiances for a given scattering angle. Plotted also are Mie calculations for monodispersed particle of different radii (Gumbel et al., 2001).

ured number density seems to be 200 cm^{-3} (Gumbel et al., 2001).

Good fits can be obtained using a lognormal distribution [e.g., $f(a)=\frac{1}{\sqrt{2\pi}\zeta a}\exp(-\ln^2(a/a_0)/2\zeta^2)$, where a_0 and $\zeta=\ln\sigma$ are parameters of the particle size distribution $f(a)$] and rectangular particle size distributions (Gumbel and Witt, 2001). In particular, it follows that data in Fig. 7 can be fitted using the lognormal size distribution with $a_0=21$ nm, $\sigma=1.4$. Therefore, the value of a_0 is about one half of the correspondent radius for monodispersed spheres (see Fig. 7) in the case studied. Note that the value of ζ is approximately equal to 0.34 at $\sigma=1.4$. This means that the coefficient of variance $\mathbb{C}\equiv\sqrt{\exp(\zeta^2)-1}$ (Kokhanovsky, 2001), which is defined as the ratio of the standard deviation of the radius to the mean radius, is equal to 0.35 for a NLC event under investigation. This is close to values of $\mathbb{C}$ observed for tropospheric clouds (Kokhanovsky, 2004).

There currently is a controversy with respect to the choice of the particle size distribution for the fitting procedure. In particular, lognormal distributions are usually observed for coagulation/coalescence mechanisms of particle growth. NLC particles size distribution are determined mostly by condensation processes (Gumbel et al., 2003). Moreover, lognormal distributions are characterized by very long tails, which should not be the case for NLCs (e.g., particles of 1 μm are hardly expected for NLCs). This fact forced Heintzenberg et al. (1978) to use the truncated lognormal distribution.

A useful single number to compare values of a in different NLC events is given by the asymmetry factor $s=p(45^\circ)/p(135^\circ)-1$. The value of s vanishes for molecular scattering, which is symmetric with respect to the scattering angle 90°. We present the dependence of s on the size of spherical ice particles at $\lambda=222$ nm in Fig. 8. The refractive index is equal to 1.37. It follows from Fig. 8 that $s=1.8$ at $a=42$ nm. This corresponds well to the measurements given by Gumbel et al. (2001) (see Fig. 7). Therefore, a single number can be used to retrieve the radius of particles. Clearly, due to statistical noise (see Fig. 7), the measurements of the full phase function are preferable. Note that a unique determination of the radius a is possible for values of $s<2.5$ This is not the case for larger values of s, however (see Fig. 8).

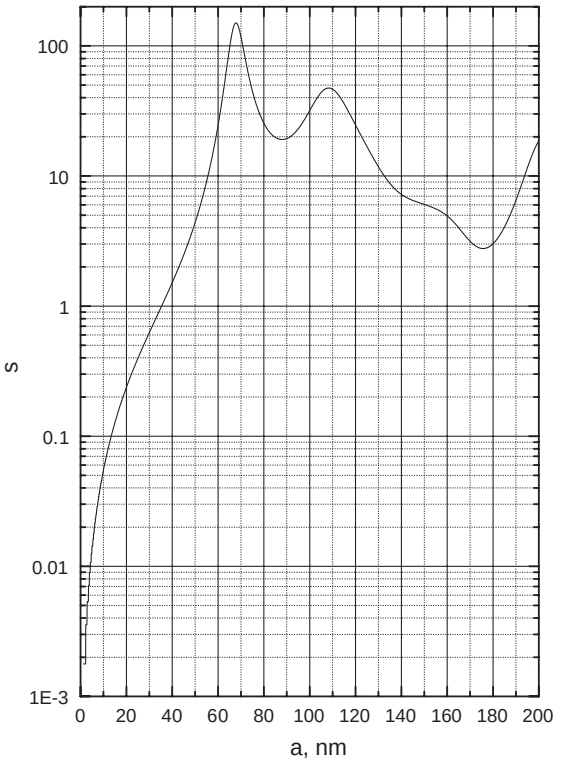

Fig. 8. The dependence of the asymmetry factor s on the radius of a spherical particle at the wavelength 222 nm. The refractive index of ice is equal to 1.37.

Yet another single number for the characterization of the size of crystals is given by the color ratio $c(\lambda_1, \lambda_2, \theta)=\sigma_S(\lambda_1, \theta)/\sigma_S(\lambda_2, \theta)$, i.e. the ratio of the angular scattering coefficients $\sigma_S(\lambda, \theta)$ (see Appendix) at two wavelengths λ_1 and λ_2 and a given scattering angle θ. We present the dependence of c (222 nm, 449 nm, $\pi/2$) on the radius of ice spheres in Fig. 9. It follows from Fig. 9 that $c\approx16$ at $a=42$ nm. This number corresponds well to the experimental value of $c=15\pm5$ obtained by Gumbel and Witt (2001) for the same NLC event as studied in Fig. 7, suggesting that radii obtained from the color ratio and the phase function are consistent. This is also the case if the polydispersed NLC is assumed (Gumbel and Witt, 2001). Therefore, the simultaneous determination of $p(\theta)$ and c does not give a clue for the selection of the right size distribution in the case studied.

The possibility of the derivation of NLC crystals dimensions from the phase function measured by a rocket-borne instrument is limited to the case of

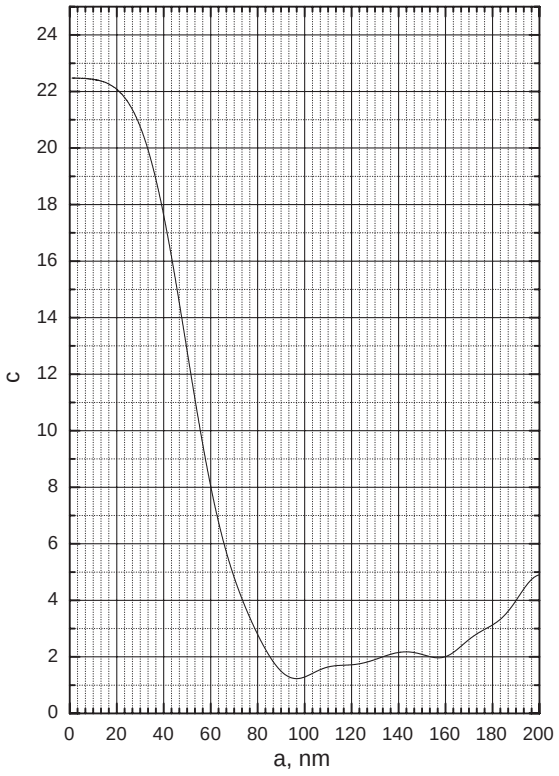

Fig. 9. The dependence of the color ratio c(222 nm, 449 nm, 90 °C) on the radius of a spherical particle.

horizontally homogeneous cloud fields, which is not always the case (see Fig. 1). Also detailed knowledge of the payload altitude at every time of measurement is needed.

Therefore, Von Cossart et al. (1999) used lidar techniques to study sizes of particles in NLCs. In particular, they have measured color ratios $c_1 \equiv c$ (1064 nm, 532 nm, π) and $c_2 \equiv c$ (355 nm, 532 nm, π) in the backward direction. Experimental results scatter in the range 0.06–0.2 for c_1 and 0.5–3.5 for c_2. We have presented color ratios c_1, c_2 obtained using Mie theory for monodispersed spheres in Fig. 10. As we see, the dispersion of experimental data cannot be explained by light scattering theory for monodispersed spheres. This also follows from Figs. 11 and 12. Therefore, the scattering by polydispersed or nonspherical particles should be used to explain the phenomenon. In particular, Von Cossart et al. (1999) used Mie theory for polydispersed spheres to explain results obtained.

The value of σ in the lognormal PSD seems to be in the range 1.2–1.45 with the most probable value being 1.42. This means that the coefficient of variance $\mathbb{C}$ of the particle size distribution varies in the range 0.18–0.37 with the most probable value being 0.35. We see that size distributions of crystals in noctilucent clouds are rather narrow. In particular, size distributions of particles in stratosphere have almost two times larger values of $\mathbb{C}$ ($\approx$60% (Kokhanovsky, 2001)).

The value of a_0 was in the range 19–69 nm, depending on the sounding time. The average value of a_0 was 51 nm. We have found that for such small values of a_0, the values of c_1, c_2 almost do not depend on shape effects. This is an important point.

Von Cossart et al. (1999) also retrieved the number concentration N of particles in the unit volume of NLC. The value of N strongly depends on the size of particles and varies in the range 23–1078 cm^{-3} with average value of 82 cm^{-3}.

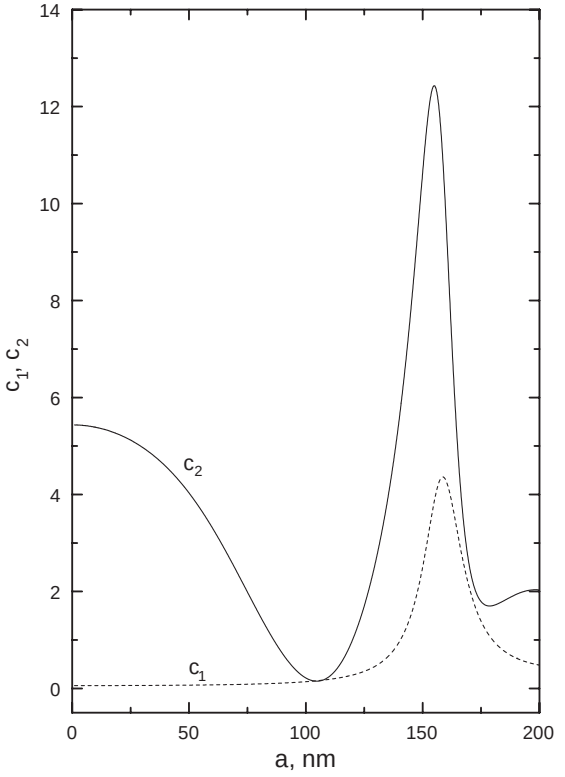

Fig. 10. The dependence of color ratios $c_1 \equiv c$(1064 nm, 532 nm, π) and $c_2 \equiv c$ (355 nm, 532 nm, π) on the size of ice spheres.

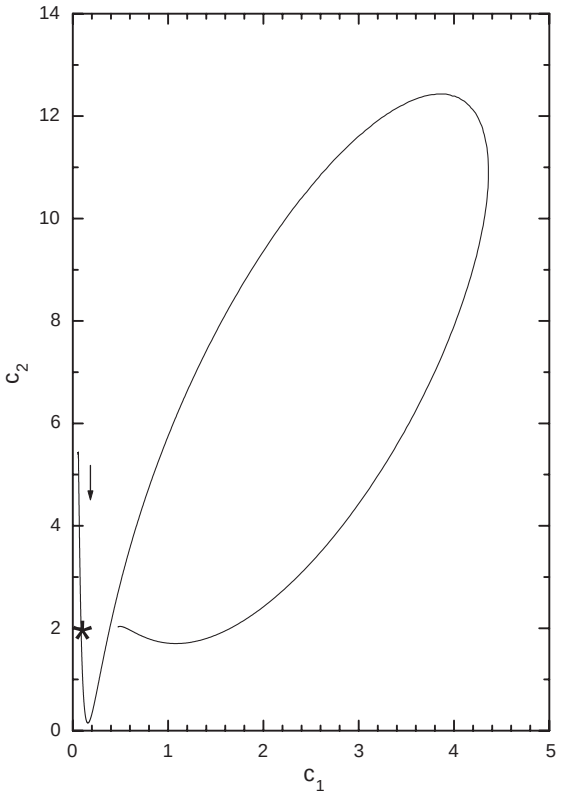

Fig. 11. The dependence of c_2 on c_1. The approximate position of measurements performed by Von Cossart et al. (1999) is given by a star. The arrow shows the direction of the increase of the dimension of ice spheres.

We see that the combination of three wavelengths in the backward direction allows for the determination of particle size distribution parameters (e.g., the pair (a_0, σ)). Clearly, still larger number of wavelengths and broader spectral range studied will enhance the accuracy of the retrieval. Alpers et al. (2000) have used five color lidar observations of NLC at 54°N. The following values of a_0 and σ give the best fit of their measurements: a_0=27.5 nm, σ=1.5. This result was obtained using the minimization technique based on measurements of backscattering at 355 nm, 393 nm, 423 nm, 532 nm, and 770 nm. Interestingly, the last wavelength (770 nm) did not produce significant backscattering in a single lidar experiment reported by Alpers et al. (2001) (although the NLC signal was detected at wavelengths 393 nm, 423 nm, and 532 nm on the same occasion). The reason for this remains unclear.

It was shown above that spectral measurements of the angular scattering coefficient in the backward direction are very informative in respect to optical particle sizing problems. It could be of interest to use also spectral measurements of angular scattering coefficient for other scattering directions. This is difficult to achieve from ground-based techniques because of the interference of atmospheric layers below NLCs. It is difficult to account for them if one uses standard ground-based spectrophotometric techniques. Note that lidar systems allow to study a signal from a given height, thereby minimizing interference from other atmospheric layers.

Yet another possibility to minimize the influence of the Earth's albedo effects and tropospheric scattering is to use an optical instrument on the orbiting satellite (Kondratyev et al., 1971). In particular, one can use spectral channels with $\lambda \leq 315$ nm. There is no contribution to the signal

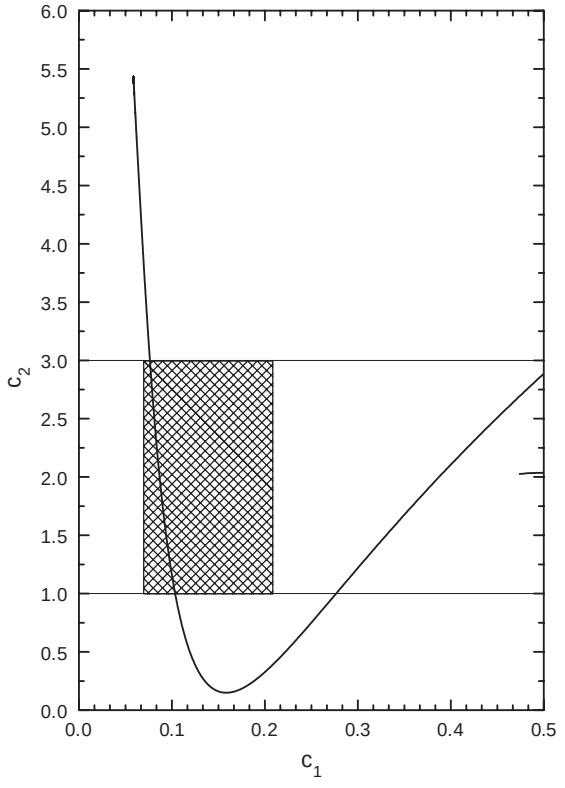

Fig. 12. The same as in Fig. 11 but with a higher resolution for values of $c_1 < 1/2$. The dashed line gives the approximate position of measured results.

from the ground at such small wavelengths due to gaseous absorption (see Fig. 6). Then the well-known Rayleigh scattering contribution (Bates, 1984; Bucholtz, 1995) should be removed from the signal, which is a straightforward procedure. The correspondent analysis has been performed by Von Savigny et al. (2004) using space-borne spectrometer data. The characteristic example is shown in Fig. 13. We see that monodispersed spheres with radii 80 nm, 92 nm, and 95 nm well represent spectral measurements. For polydispersions having the lognormal distributions, correspondent values of a_0 were approximately one half as large (at $\sigma=1.4$). Similar results using spectrographic imagers on the Midcourse Space Experiment satellite were obtained by Carbary et al. (2002), who reported values of $a_0=65.2$ nm and $\sigma=1.15$ derived from the spectral scattered light intensity in the range 200–300 nm. They also emphasized that spectra above 315 nm are contaminated by the Earth albedo effects (see Fig. 6).

The scattered light intensity I_{sca} depends on the wavelength as a power law: $I_{sca}=\beta\lambda^{-\alpha}$, where β is spectrally neutral constant and α depends on the NLC event studied. Von Savigny et al. (2004) found values of α in the range 2.0–3.0. Carbary et al. (2002) report similar results with α in the range 1.0–2.0.

The results of calculation of the index α as the function of the parameters a_0 and σ using the Mie theory for spherical polydispersions are given in Fig. 14 at $\theta=39^\circ$ and $\lambda=240$–280 nm. Fig. 14 (and similar figures for other θ) can be used for the conversion of α to the pair (a_0, σ) for instruments capable of measuring light scattering in the spectral range 240–280 nm, where the contamination of NLC signal by background light (e.g., from below) is small (see Fig. 6). Then the value of σ should be a priori assumed.

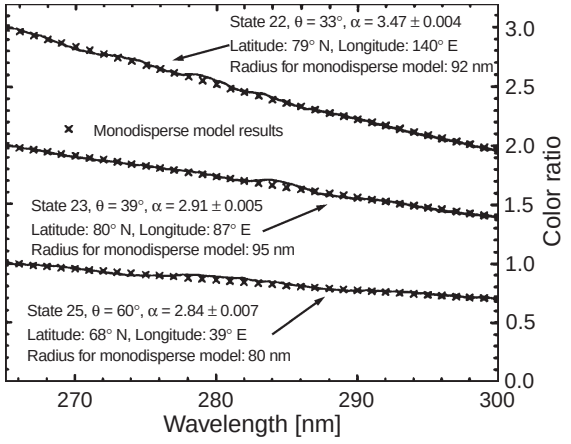

Fig. 13. Spectral color ratios $c(\lambda, 265\text{ nm})$ obtained from measurements (solid lines) and Mie calculations (crosses) using the monodispersed spherical model of scatterers (scaled by a factor of 2 for state 23 and 3 for state 22 to allow a better discrimination of different spectra (Von Savigny et al., 2004).

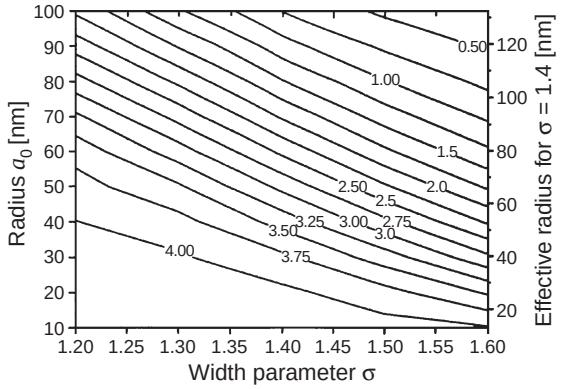

Fig. 14. Theoretical dependence of the spectral exponent α on the lognormal particle size distribution parameters within the 265–300 nm spectral window for scattering angle $\theta=39^\circ$ obtained using Mie theory for spherical polydispersions (Von Savigny et al., 2004).

Summing up, we present values of particle radii in NLCs obtained in recent experiments in Table 2. We see that the average value of a_0 is close to 35 nm, which is well inside of the variability of the radius of particles in NLCs derived in earlier works (Avaste et al., 1980; Thomas and McKay, 1985). We also give the effective radius $a_{ef}=a_0\exp(-2.5\ \ln^2\sigma)$ (Kokhanovsky, 2001) and the coefficient of variance of the particle size distribution $\mathbb{C}=\sqrt{\exp(\ln^2\sigma)-1}$ ($\approx\ln\sigma$ as $\sigma\rightarrow1.0$) in the same table. Their meaning is more transparent as compared to the pair (a_0, σ). In particular, $a_{ef}=3V/S$, where V is the average volume of particles and S is their surface area. Optical properties of spherical polydispersions are mostly governed by the value of the effective radius a_{ef} (Kokhanovsky, 2001). It follows that the average value of the pair $(a_{ef}, \mathbb{C})$ in Table 2 is (52 nm, 0.32). These parameters can be used as first guess parameters in inversion schemes to retrieve the pair $(a_{ef}, \mathbb{C})$ in noctilucent clouds.

We see, therefore, that the average effective diameter of particles found in recent experiments is

Table 2
The parameters a_0,σ of the lognormal particles size distribution in NLCs according to different measurement techniques

Author	a_0, σ	a_{ef}, $\mathbb{C}$	Measurement technique
Von Cossart et al. (1999)	a_0=51 nm, σ=1.42 (average values)	a_{ef}=65 nm, $\mathbb{C}$ = 0.35	Lidar spectral measurements
Alpers et al. (2000)	a_0=27.5, σ=1.5	a_{ef}=41 nm, $\mathbb{C}$ = 0.42	Lidar spectral measurements
Gumbel et al. (2001)	a_0=21 nm, σ=1.4 (a=42 nm)	a_{ef}=28 nm, $\mathbb{C}$ = 0.35	Rocket-borne angular measurements
Carbary et al. (2002)	a_0=65 nm, σ=1.15 (average values)	a_{ef}=68 nm, $\mathbb{C}$ = 0.14	Space-borne spectral measurements
Von Savigny et al. (2004)	a_0=45 nm, σ=1.4 (a=90 nm)	a_{ef}=60 nm, $\mathbb{C}$ = 0.35	Space-borne spectral measurements

Radius a of the monodispersed model is also given in selected cases.

close to 100 nm and the standard deviation of the particle size distribution is approximately $\langle a\rangle/3$, where $\langle a\rangle$ is the average radius of particles.

Comparison of data obtained from limb scanning instruments such as the Wind Imaging Interferometer and the Solar Mesospheric Explorer with data obtained from the solar occultation measurements (Polar Ozone and Aerosol Measurement experiment) for NLC events is presented by Shettle et al. (2002). They found a trend in cloud brightness with time. Similar results were reported by Klostermeyer (2002). Brighter (therefore, larger a_{ef}, N) and more frequently occurred clouds are observed in recent years. However, this conclusion should be verified in future using (if possible) a single optical instrument, thereby avoiding possible biases related to different measurement modes.

3. The shape of crystals

The shape of ice crystals can influence light scattering characteristics considerably (Gadsden, 1977a; Mishchenko, 1991). To show this we have calculated the phase function and normalized phase matrix elements (see Appendix A) for volume-equivalent spheres, cubes, and hexagonal cylinders. It was assumed that λ=270 nm and a=80 nm. Then the size parameter $2\pi a/\lambda$ is 1.86. The refractive index of ice was taken as 1.34. Calculations for all particles have been carried out using the discrete dipole approximation (DDA) code freely available over Internet (see Appendix B). The random orientation of particles has been assumed. This assumption is valid due to the fact that aerodynamic forces are weak at heights where NLCs are observed. Also both magnetic and electrical alignment are ruled out (Bohren, 1983). Note that we have checked the DDA results for spheres by Mie calculations. A good agreement (within 1%) has been found.

Let us consider results obtained. The calculated phase functions are given in Fig. 15a. We see that phase functions for all shapes are close to each other for scattering angles smaller than 120°. This can explain the successful application of Mie theory to phase functions of NLCs by Gumbel et al. (2001) and Gumbel and Witt (2001) using Mie theory (see Fig. 7). It appears that the asymmetry ratio s depends on the shape of particles. Generally, the sensitivity of the phase function to the shape greatly increases in the range of scattering angles larger than 120°. So it could be of advantage to define s for angles 45 and 115°. Then shape effects are not of great importance, as one can deduce from Fig. 15a.

It is known that shape considerations do not enter into estimates of the amount of scattering per unit volume of scattering particles within the framework of Rayleigh theory (Bohren, 1983). It is often believed that this is approximately correct also for sizes just above the Rayleigh limit (Bohren, 1983; Thomas and McKay, 1985). This, however, depends on the angular and spectral range studied (see Fig. 15a) and can

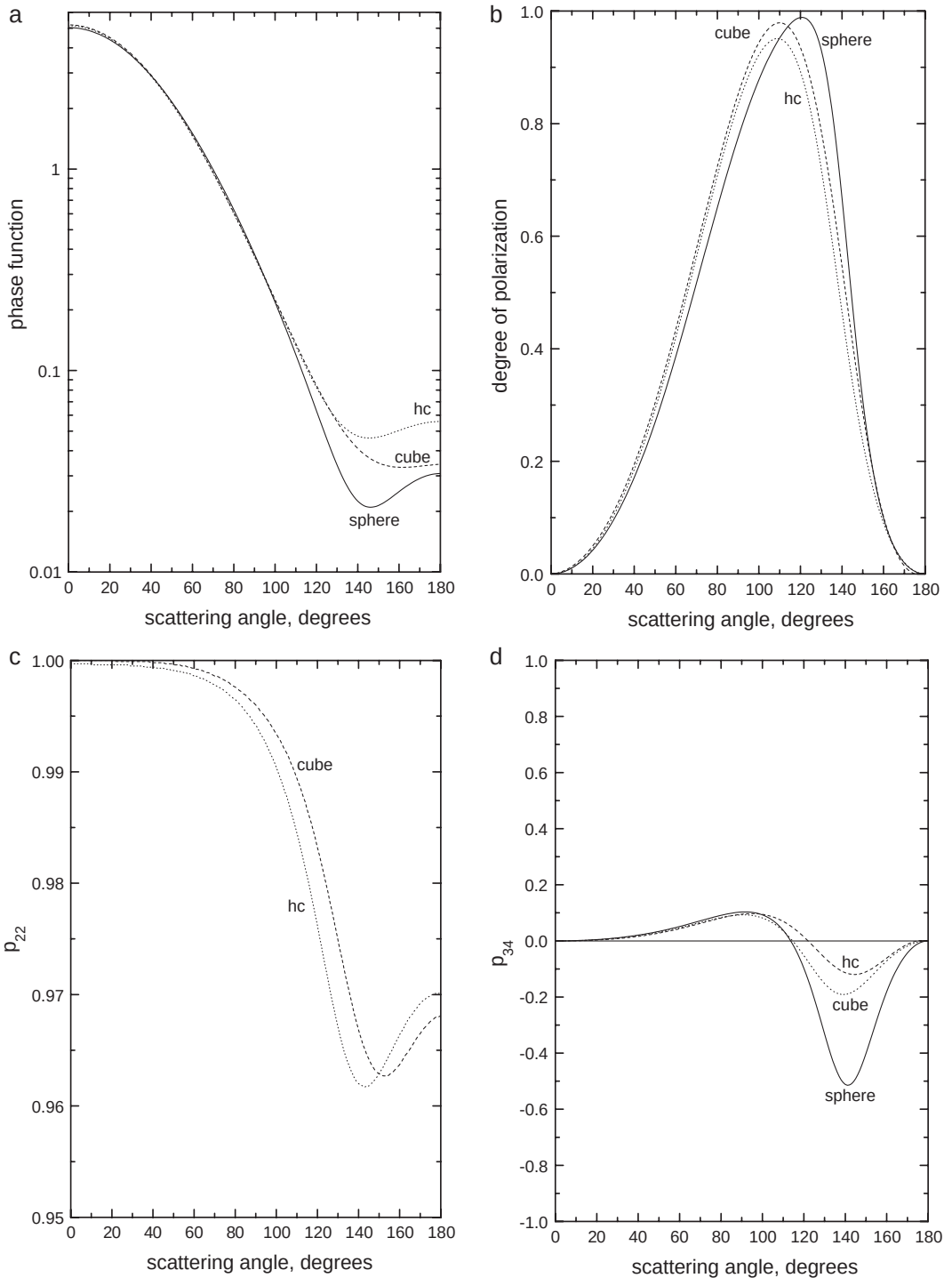

Fig. 15. The phase function (a), the degree of polarization (b), and elements of the normalized phase matrix (c, d, e) for spherical particles with the radius 80 nm at the wavelength 270 nm ($n = 1.34$). The results for cubes and hexagonal cylinders (hc) having the same volume as a sphere are also shown. The length of the cylinder is equal to the side of the hexagonal cross section.

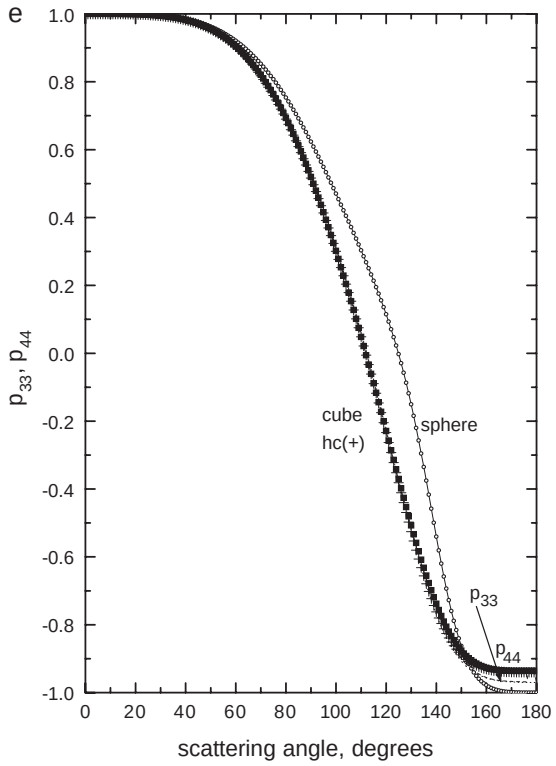

Fig. 15 (*continued*).

potentially lead to biases in sizes retrieved using backscattering techniques. Note that shapes given in Fig. 15a are compact. Differences increase if we consider elongated particles or thin plates (Mishchenko, 1991). However, there are no physical arguments for such shapes to exist in NLCs. In particular, laboratory experiments confirm that formation of equidimensional crystals, such as hexagons and cubes, is favoured at low temperatures (Turco et al., 1982; Roddy, 1986; Svanberg et al., 1998). This, however, is in contrast with interpretation of results obtained from lidar measurements performed by Baumgarten et al. (2002), who found that their measurements can be explained by the chaotically oriented needles having the ratio of the length to the diameter around 10 or oriented needles having this ratio equal to 5. This contradiction should be explored in a future research. In particular, there were no mechanism proposed that can explain oriented or needle/plate-like particles in NLCs.

Color ratios for such small particles as those in NLCs do not depend on shape effects very much. This is due to the fact that the form-factors are approximately cancelled in such ratios. Therefore, color ratios cannot be used to study the shape of crystals in NLCs. Then the polarimetric techniques should be used.

Differences in optical characteristics of particles are much more pronounced if the polarization characteristics of scattered light are considered (Kokhanovsky, 2003). Therefore, it is of importance to study not only the phase function but also the scattering matrix $\hat{\mathbf{P}}$ (see Appendix A), which relates Stokes vectors of incident and scattered light beams.

Let us consider now the influence of the shape of particles on the elements of the normalized scattering matrix (see Fig. 15) $\hat{\mathbf{p}}(\theta)=\hat{\mathbf{P}}\,\theta)/p(\theta)$, where $p(\theta)$ is the phase function.

The elements of this matrix have the following physical meaning (Kokhanovsky, 2003):

- $-p_{12}$ is the degree of polarization of scattered light for the solar light illumination;

- p_{44} is the degree of circular polarization of scattered light for the illumination by right-hand circularly polarized light;
- p_{34} is the degree of circular polarization of scattered light for the illumination by linearly polarized light with azimuth -45°.

The element p_{22} is equal to one for spheres. So its deviation from one is the measure of nonsphericity. The same applies to the difference $\Delta = p_{44} - p_{33}$, which is exactly zero for spheres. Note that the lidar cross polarization ratio is given by $\Delta = (1 - p_{22})/(1 + p_{22})$. It refers to the ratio of the intensities for the vertical registered polarization in the case of the emitted horizontally polarized light to that of the vertical registered polarization for the same emission conditions.

We present the angular dependence of the degree of polarization $(-p_{12})$ in Fig. 15b both for nonspherical particles and for spheres. It follows that the degree of polarization by nonspherical particles is generally closer to that of Rayleigh scattering. It means, in particular, that the interpretation of measurements using Mie theory (see, e.g., Fig. 5) may underestimate the size of particles. The possibility of such an underestimation was first found by Mishchenko (1991), who used the model of ellipsoidal particles. The largest differences are around the scattering angle 140° (as in Fig. 15a). Small differences take place at small scattering angles.

The element p_{22} is given in Fig. 15c. Its value (if measured in NLC) can be as small as 0.96 for nonspherical particles considered here. Such a small deviation from one is possible to measure, however. This was demonstrated by Baumgarten et al. (2002), who measured the value of Δ at exact backward scattering direction and found that it is in average equal to $(1.7 \pm 1.0)\%$ at the wavelength 532 nm. It is interesting that the values of Δ differ inside the NLC. It means that the size/shape of particles changes with height. The measured values of Δ (see Fig. 16) are lower in that area of NLC where particles have largest concentrations. It is larger in the upper part of the cloud.

We have calculated the value of Δ for cubic particles at the backward direction and $\lambda = 532$ nm. Data for different sizes are given in Fig. 16. We see that measurements of Baumgarten et al. (2002) can be explained by the presence of rather small cubic crystals in the middle of the NLC event studied. Values of Δ larger than 0.7% correspond to cubes having sizes larger than 160 nm (see Fig. 16). The maximal values of measured Δ ($\approx 3.4\%$) cannot be explained in the framework of the cubic particles model at sizes smaller than 350 nm. Such large values of Δ are due to either larger sizes of particles in comparison with those studied in Fig. 16 or due to needle-like particles (see, e.g., Baumgarten et al., 2002). However, neither the existence of needles in NLCs nor their peculiar vertical distribution with smaller particles in the core of NLC has been explained on the grounds of possible NLC formation mechanisms. Moreover, experimental data presented by Gumbel and Witt (1998) show that sizes can change on the scale length 1 km with larger sizes closer to the base of NLCs.

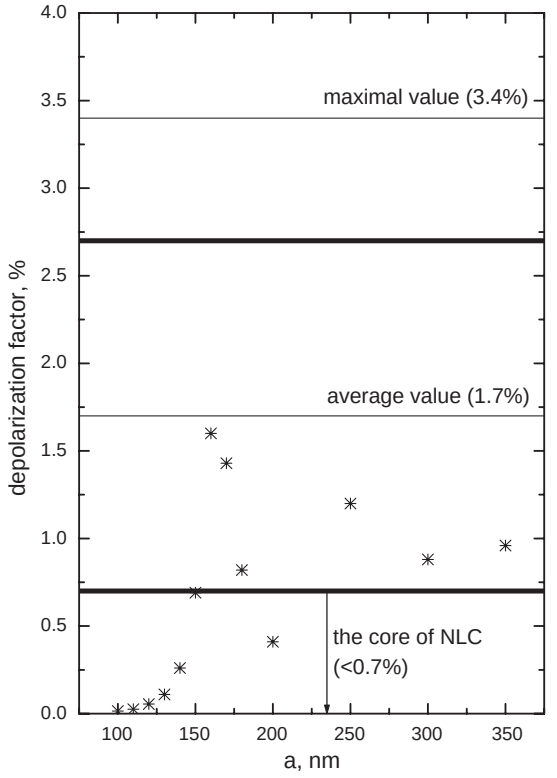

Fig. 16. The lidar depolarization ratio Δ for cubic monodispersed particles having the random orientation at the wavelength 532 nm. Results of measurements (Baumgarten et al., 2002) are also given. The value of Δ is equal to zero for spherical particles.

Let us consider now the matrix element p_{34}. The deviations between different particle models are quite strong for the scattering angle 140°, if the value of p_{34} is measured (see Fig. 15d). This can be used to identify

the shape of particles. The element p_{34} gives the strength of the transition of the linearly polarized light into the circular polarization mode as outlined above. Therefore, such a transition is of importance around the scattering angle 140°. It was found that light coming from NLCs can have a circularly polarized component (Gadsden, 1977b; Gadsden et al., 1979). The origin of this effect is not clear. However, comparatively large values of p_{34} around the scattering angle 140° may cause the transformation of the scattered linearly polarized light from areas outside of NLCs to the circularly polarized mode. This question should be clarified in further research, however.

The elements p_{33}, p_{44} for hexagonal particles, cubes, and spheres are given in Fig. 15e. They coincide for spheres. They almost coincide for cubes and hexagonal cylinders, being closer to a correspondent Rayleigh curve ($p_{44}=2\cos\theta/(1+\cos^2\theta)$) (Kokhanovsky, 2001)).

Overall, our analysis shows that nonspherical NLC particles can give large deviations in the scattering matrix (including phase function) as compared to spheres of the same volume. In particular, nonspherical scattering produces more Rayleigh-like scattering behaviour, which led to underestimation of the size of particles in NLCs if the spherical model is used in the retrieval procedure.

On the other hand, the sensitivity of light scattering to the shape of particles can be in principle used for their shapes retrieval. However, then the problem of the ambiguity arises. Several shapes/size combinations can satisfy the same optical data. This also is a problem for tropospheric ice clouds, but the various imaging techniques used in cirrus cloud microphysics studies (Heymsfield, 1986) currently are not available for the investigation of NLCs. Laboratory experiments, however, can provide some clues to the possible range of shapes (see, e.g., Svanberg et al., 1998). Therefore, a major effort should be put in this direction.

4. Conclusions

We reviewed here a number recent rocket-borne, satellite and lidar measurements to retrieve the size/shape information of NLC particles. Derived values of a_0 were in the range 21–65 nm. This approximately corresponds to radii $a=42$–125 nm of the monodispersed NLCs. These values are inside the variability reported in some earlier works. However, recent experiments tend to give lower values than those obtained in earlier works. For instance, Avaste et al. (1980) claimed that $a \approx 150$ nm on average. Therefore, more investigations are needed (preferably, using particle collectors). Note that techniques based on different spectral regions may produce different values of a due to the effect of different sensitivity to the dimension of crystals. In particular, there is a tendency to retrieve larger sizes for visible wavelengths than for UV-measurements. Indeed, UV-measurements are sensitive to much greater fraction of the total particle population (Thomas, 1991).

Even less is known about the shape of particles than about their size. Lidar measurements show that particles depolarize backscattering light. So scatterers clearly have nonspherical shapes. Taking into account their small size, the observed depolarization in the area above a core of NLC can be explained using the hypothesis of needle-shaped particles. However, the formation mechanism for such shapes is still lacking. Cubic ice, which may exist in NLCs, would explain the results of the depolarization ratio Δ below 0.7% as it was shown above. However, the cubic model cannot describe values of $\Delta \approx 3.4\%$ in the area above the NLC core. This result is somewhat puzzling.

Summing up, in spite of 120 years of NLC-related research major questions in respect to properties of noctilucent (or polar mesospheric) clouds remain to be answered. In particular, we do not understand what are the most important initial condensation nuclei. What is the shape of ice crystals? What is their most typical size? Do we have mono-modal or multi-modal (Carbary et al., 2004) size distributions of crystals in NLCs? Is there indeed a substantial trend in the NLCs' brightness and frequency of occurrence? And above all—do changes in NLCs serve as a harbinger of climatic change?

Answers to these and some other questions related to NLCs (see, e.g., Thayer et al., 2003) will be the major focus of mesospheric physics in coming years. Laboratory and in situ experiments should be considered as main avenues of attack of this important but very complex problem.

A goal of this review is to attract more attention and research efforts to atmospheric physics and chemistry across the summer polar mesopause.

Acknowledgements

This work was funded by the BMBF via GSF/PT-UKF (07UFE12/8). The author is grateful to C. von Savigny and G. Witt for insightful discussions on the subject of noctilucent clouds. He thanks B. Draine for the possibility to use his DDA code and to J. Miao for clearing some important issues related to the DDA code performance and settings.

Appendix A. Mie theory

Mie theory (Van de Hulst, 1981; Kokhanovsky, 2001) allows calculations of the intensity and polarization characteristics of light scattered by a single spherical particle characterized by the arbitrary complex relative refractive index m. In order to simplify the notation we assume that the surrounding medium is vacuum.

The scattered light intensity can be presented in the following form:

$$I = \frac{i_1 + i_2}{2k^2r^2} I_0,$$

where I_0 is the incident light intensity, r is the distance to the observation point, $k=2\pi/\lambda$, λ is the wavelength. The dimensionless functions i_1 and i_2 are found as follows:

$$i_1=|S_1|^2,\ i_2=|S_2|^2,$$

where

$$S_1(\theta) = \sum_{n=1}^{\infty} \frac{2n+1}{n(n+1)} \{a_n\tau_n(\cos\theta) + b_n\pi_n(\cos\theta)\},$$

$$S_2(\theta) = \sum_{n=1}^{\infty} \frac{2n+1}{n(n+1)} \{a_n\pi_n(\cos\theta) + b_n\tau_n(\cos\theta)\}$$

and

$$\pi_n(\cos\theta) = \frac{P_n^{(1)}(\cos\theta)}{\sin\theta}, \quad \tau_n(\cos\theta) = \frac{\mathrm{d}P_n^{(1)}(\cos\theta)}{\mathrm{d}\theta}.$$

The amplitude coefficients are given as:

$$a_n = \frac{\psi_n'(y)\psi_n(x) - m\psi_n(y)\psi_n'(x)}{\psi_n'(y)\xi_n(x) - m\psi_n(y)\xi_n'(x)},$$

$$b_n = \frac{m\psi_n'(y)\psi_n(x) - \psi_n(y)\psi_n'(x)}{m\psi_n'(y)\xi_n(x) - \psi_n(y)\xi_n'(x)}.$$

Here $y=mx$, $x=ka$, where a is the radius of a sphere. Also we have for special functions involved: $\psi_n(x) = \sqrt{\frac{\pi x}{2}} J_{n+\frac{1}{2}}(x)$, $\xi_n(x) = \sqrt{\frac{\pi x}{2}} H^{(2)}_{n+\frac{1}{2}}(x)$, $J_{n+\frac{1}{2}}$ and $H^{(2)}_{n+\frac{1}{2}}$ are Bessel and Hankel functions, $P_n^{(1)}(\cos\theta)$ is the associated Legendre polynomial, θ is the scattering angle. Primes denote derivatives.

Expressions for the values of the extinction efficiency $Q_{\mathrm{ext}} = C_{\mathrm{ext}}/\pi a^2$, scattering efficiency $Q_{\mathrm{sca}} = C_{\mathrm{sca}}/\pi a^2$, the phase function $p(\theta)$ at the natural light illumination, and the asymmetry parameter $g = \frac{1}{2}\int_0^{\pi} p(\theta)\sin\theta\cos\theta\,\mathrm{d}\theta$ are presented in Table A1. Here C_{sca} is the scattering cross section and C_{ext} is the extinction cross section.

It follows for polydispersed media having the particle size distribution $f(a)$:

$$\sigma_{\mathrm{ext}} = N\int_0^{\infty} \pi a^2 Q_{\mathrm{ext}} f(a)\mathrm{d}a,$$

$$\sigma_{\mathrm{sca}} = N\int_0^{\infty} \pi a^2 Q_{\mathrm{sca}} f(a)\mathrm{d}a,$$

$$p(\theta) = \frac{2\pi N\int_0^{\infty} (i_1 + i_2) f(a)\mathrm{d}a}{k^2\sigma_{\mathrm{sca}}},$$

$$g = \frac{\int_0^{\infty} \pi a^2 Q_{\mathrm{sca}}\, p(\theta) f(a)\mathrm{d}a}{\int_0^{\infty} a^2 Q_{\mathrm{sca}}\, f(a)\mathrm{d}a}.$$

Here σ_{ext} and σ_{sca} are extinction and scattering coefficients, N is the number of particles in a unit volume of a scattering medium. One can also introduce the angular scattering coefficient:

$$\sigma_{\mathrm{sca}}(\theta) = \frac{N\int_0^{\infty} (i_1 + i_2) f(a)\mathrm{d}a}{2k^2}.$$

Table A1
Light scattering characteristics of isotropic spheres

Value	Formula
Q_{ext}	$\frac{2}{x^2}\sum_{n=1}^{\infty}(2n+1)Re(a_n+b_n)$
Q_{sca}	$\frac{2}{x^2}\sum_{n=1}^{\infty}(2n+1)\left[\lvert a_n\rvert^2+\lvert b_n\rvert^2\right]$
$p(\theta)$	$\frac{2(i_1+i_2)}{x^2Q_{sca}}$
g	$\frac{4}{x^2Q_{sca}}\sum_{n=1}^{\infty}\left[\frac{n(n+2)}{n+1}Re(a_na_{n+1}^*+b_nb_{n+1}^*)+\frac{2n+1}{n(n+1)}Re(a_nb_n^*)\right]$

Then it follows:

$$\sigma_{sca}=2\pi\int_0^{\pi}\sigma_{sca}(\theta)\sin\theta d\theta.$$

Amplitude functions S_1 and S_2 determine the elements of the normalized scattering matrix $\hat{\mathbf{p}}(\theta)=\hat{\mathbf{P}}(\theta)/p(\theta)$, where

$$\hat{\mathbf{P}}(\boldsymbol{\theta})=p(\boldsymbol{\theta})\begin{pmatrix}1 & p_{12}(\boldsymbol{\theta}) & 0 & 0\\ p_{12}(\boldsymbol{\theta}) & p_{22}(\boldsymbol{\theta}) & 0 & 0\\ 0 & 0 & p_{33}(\boldsymbol{\theta}) & p_{34}(\boldsymbol{\theta})\\ 0 & 0 & -p_{34}(\boldsymbol{\theta}) & p_{44}(\boldsymbol{\theta})\end{pmatrix},$$

and $p_{12}=(i_1-i_2)/(i_1+i_2)$, $p_{22}=1$, $p_{33}=p_{44}=\mathrm{Re}(S_1S_2^*)/(i_1+i_2)$, $p_{34}=\mathrm{Im}(S_1S_2^*)/(i_1+i_2)$ for spheres (Kokhanovsky, 2003). Stars denote conjugated values.

Appendix B. The discrete dipole approximation

Optical properties of particles with sizes comparable to or smaller than the light wavelength can be calculated within the framework of the discrete dipole approximation (DDA). Then a particle of any shape is replaced not just by a single dipole, as it is in the case of the Rayleigh approximation, but by means of an array of N ($N\rightarrow\infty$) point dipoles, with the spacing between dipoles small compared to the wavelength. This replacement requires specification of both geometry (location $\vec{r}_j$ of the dipoles $j=1,\ldots,N$) and the dipole polarizabilities α_j. Note that for a finite array of point dipoles the scattering problem can be solved exactly (Purcell and Pennypacker, 1973; Bohren and Singham, 1991). This approach makes it possible to consider spherical and nonspherical particles with characteristic sizes $a\sim\lambda$ (λ is the wavelength) and smaller. For larger particles numerical calculations become unstable.

Each dipole has an oscillating polarization in response to both an incident plane wave and electric fields due to all other dipoles in an array. This is why the DDA is also sometimes referred to as the coupled dipole approximation. The dipole at location $\vec{r}_i$ acquires a dipole moment:

$$\vec{p}_i=\alpha_i\vec{E}_i, \tag{1}$$

where α_i is the polarizability of an dipole i. The electric field $\vec{E}_i$ is due to the incident field $\vec{E}_{inc}=\vec{E}_0\exp(-(\vec{k}\vec{r}_i-\omega t))$ ($\vec{k}=k\vec{n}$, $k=2\pi/\lambda$, $\vec{n}$ is the unit vector in the direction of wave propagation, t is time and ω is frequency) at the point with the radius-vector $\vec{r}_i$ and contributions from dipoles with amplitudes $\vec{p}_j$, located at points $\vec{r}_j$. Thus, according to the linear superposition principle, one obtains for the electric field $\vec{E}_i$ at the point $\vec{r}_i$, where i-dipole is located:

$$\vec{E}_i=\vec{E}_{inc}+\vec{E}, \tag{2}$$

where $\vec{E}=\sum_{j\neq i}^{N}\vec{E}_j$ is the sum of fields from all dipoles except the dipole with the radius-vector $\vec{r}_i$. The electric field, in vacuum, of a dipole with the amplitude $\vec{p}_i$, evaluated at the distance $r_{ij}=|\vec{r}_i-\vec{r}_j|$ has the following analytical form:

$$\vec{E}_i=\frac{\exp(-i(kr_{ij}-\omega t))}{r_{ij}}\times\left[\frac{1+ikr_{ij}}{r_{ij}^2}\left(\frac{3(\vec{p}_j\cdot\vec{r}_{ij})\vec{r}_{ij}}{r_{ij}^2}-\vec{p}_j\right)-k^2\left(\frac{(\vec{p}_j\cdot\vec{r}_{ij})\vec{r}_{ij}}{r_{ij}^2}-\vec{p}_j\right)\right]. \tag{3}$$

It should be pointed out that the sum $\sum_{j\neq i}^{N}\vec{E}_j$ can be replaced by the integral (Rouleau and Martin, 1993; Stephens, 1994):

$$\vec{E}(\vec{\rho}) = \int_V \frac{\exp\left[-i\left(\vec{k}\vec{r}-\omega t\right)\right]}{r} \times\left[\frac{1+ikr}{r^2}\left(\frac{3\left(\vec{P}\cdot\vec{r}\right)\vec{r}}{r^2}-\vec{P}\right) - k^2\left(\frac{\left(\vec{P}\cdot\vec{r}\right)\vec{r}}{r^2}-\vec{P}\right)\right]d^3\vec{r}, \quad (4)$$

where $\vec{r}=\vec{\rho}-\vec{\rho}', \vec{\rho}'\neq\vec{\rho}$ and V is the volume of a particle. Eq. (3) follows from this equation after replacement of a particle by a cubic array of point dipoles, each of which has the dipole moment $\vec{p}=\vec{P}\Delta V$, where ΔV is the small volume, associated with each dipole.

Let us substitute Eqs. (2) and (3) into Eq. (1). Then it follows:

$$\vec{p}_i = \alpha_i^{-1}\exp(i\omega t)\left[\vec{E}_0\exp\left(-i\vec{k}\vec{r}_i\right) + \sum_{j\neq i}^{N}\frac{\exp\left(-ikr_{ij}\right)}{r_{ij}^3}\left(k^2\left(\vec{r}_{ij}\times\vec{p}_j\right)\times\vec{r}_{ij} + \frac{1+ikr_{ij}}{r_{ij}^2}\left(3\left(\vec{p}_j\cdot\vec{r}_{ij}\right)\vec{r}_{ij}-\vec{p}_j r_{ij}^2\right)\right)\right], \quad (5)$$

where $\vec{r}_{ij}=(\vec{r}_i-\vec{r}_j)/|\vec{r}_i-\vec{r}_j|$. The system of 3N complex Eq. (5) allows us to find the dipole moments $\vec{p}_i$ of each single dipole in the array at points $\vec{r}_j$. These points should be specified before calculations are performed. Generally speaking, the more points are chosen, the more correct results are obtained. However, the numerical solution of Eq. (5) becomes numerically unstable as $N\rightarrow\infty$. This does not allow consideration of values N larger than 10^6 at the moment. This imposes limitations on the size of particles which can be studied in the framework of the discrete dipole approximation. Yet another problem is related to the correct choice of α_i in Eq. (5) (see, e.g., Draine and Flatau, 1994).

The calculation of light scattering and absorption characteristics of known dipole moments p_j is rather simple. For instance, the electric field $\vec{E}_s$ in the far field zone is given by (Kokhanovsky, 2003):

$$\vec{E}_s = \vec{f}_s\frac{\exp\left(-i\left(\vec{k}\vec{r}-\omega t\right)\right)}{r}, \quad (6)$$

where (Draine, 1988):

$$\vec{f}_s = k^2\sum_{j=1}^{N}e^{ik\vec{r}\vec{r}_j}\left(\hat{r}\cdot\hat{r}-\hat{I}\right)p_j, \quad (7)$$

where $\hat{r}=\vec{r}/r, r=|\vec{r}|, \hat{I}$ is the unit matrix, and $\vec{r}_j$ is the unit radius-vector of a dipole located at j-position.

It follows in the framework of the DDA for the extinction and absorption cross sections (Draine and Flatau, 1994):

$$C_{ext} = \frac{4\pi k}{|\vec{E}_0|^2}\sum_{j=1}^{N}Im\left(\vec{E}_{0j}^{*}\vec{p}_j\right), \quad (8)$$

$$C_{abs} = \frac{4\pi k}{|\vec{E}_0|^2}\sum_{j=1}^{N}\left\{Im\left(\frac{\vec{p}_j\vec{p}_j^{*}}{\alpha_j^{*}}\right)-\frac{2}{3}k^3|\vec{p}_j|^2\right\}. \quad (9)$$

As number of dipoles $N\rightarrow\infty$, DDA represents exact results with higher and higher accuracy. For instance, Draine and Flatau (1994) found that for spheres with size parameter $x<12$ and the refractive index $m=1.33-0.01i$ the errors of calculations of values given by Eqs. (8) and (9) with the DDA are smaller than 3% at $N\leq 17{,}904$. About the same accuracy was obtained for the phase function. This accuracy is high enough for most of applications. It should be pointed out that the number of dipoles needed depends on the size of a particle. One should take into account about 10^5 dipoles at the size parameter $x=10$.

Different methods to solve a set of coupled linear equations for dipole moments at large N were introduced (Draine, 1988; Draine and Flatau, 1994) but they cannot be applied at $N>10^6$, because of lack of the stability of the solution. Therefore, this method cannot be applied for particles with the size parameter $x\geq 15$–20 at the moment. Fortunately, such large particles do not occur in NLCs. So the method is ideally suited for NLC studies.

References

Alpers, M., Gerding, M., Höffner, J., von Zahn, U., 2000. NLC particle properties from a five-color lidar observation at 54°N. J. Geophys. Res. 105 (D10), 12235–12240.

Alpers, M., Gerding, M., Höffner, J., Schneider, J., 2001. Multi-wavelength lidar observation of a strange Noctilucent cloud at Kühlungsborn, Germany (54°N). J. Geophys. Res. 106 (D8), 7945–7953.

Avaste, O.A., Fedynsky, A.V., Grechko, G.M., Sevastyanov, V.I., Willmann, Ch.I., 1980. Advances in Noctilucent cloud research in the space era. Pure Appl. Geophys. 118, 528–580.

Backhouse, T.W., 1885. The luminous cirrus cloud of June and July. Meteorol. Mag. 20, 133.

Bates, D.R., 1984. Rayleigh scattering by air. Planet. Space Sci. 32 (6), 785–790.

Baumgarten, G., Fricke, K.H., von Cossart, G., 2002. Investigation of the shape of noctilucent cloud particles by polarization lidar technique. Geophys. Res. Lett. 29 (13).

Bohren, C.F., 1983. On the size, shape, and orientation of noctilucent cloud particles. Tellus 35B, 65–72.

Bohren, C.F., Singham, S.B., 1991. Backscattering by nonspherical particles: a review of methods and suggested new approaches. J. Geophys. Res. 96 (D3), 5269–5277.

Brasseur, G., 1996. Chemistry in atmosphere. In: Dieminger, W., Hartmann, G.K., Leitinger, R. (Eds.), The Upper Atmosphere. Data Analysis and Interpretation. Springer-Verlag, Berlin.

Bucholtz, A., 1995. Rayleigh-scattering calculations for the terrestrial atmosphere. Appl. Opt. 34 (15), 2765–2773.

Carbary, J.F., Morrison, D., Romick, G.J., 2002. Particle characteristics from the spectra of polar mesospheric clouds. J. Geophys. Res. 107 (D23), 4686.

Carbary, J.F., Morrison, D., Romick, G.J., 2004. Evidence for bimodal particle distribution from the spectra of polar mesospheric clouds. Geophys. Res. Lett. 31 (L13108).

Draine, B.T., 1988. The discrete-dipole approximation and its application to interstellar graphite grains. Astrophys. J. 333, 848–872.

Draine, B.T., Flatau, P.J., 1994. Discrete-dipole approximation for scattering calculations. J. Opt. Soc. Am. 11 (4), 1491–1499.

Farlow, N.H., 1968. Electron microscope studies of particles on sampling surfaces recorded from space with sounding rockets. J. Geophys. Res. 73, 4363–4371.

Farlow, N.H., Ferry, G.V., 1972. Cosmic dust in the mesosphere. Space Res. 12, 369–380.

Farlow, N.H., Ferry, G.V., Blanchard, M.B., 1970. Noctilucent cloud particle studies. J. Geophys. Res. 75, 6736–6750.

Gadsden, M., 1977a. The scattering of sunlight from noctilucent cloud particles. Ann. Geophys. 33 (3), 357–362.

Gadsden, M., 1977b. The polarization of noctilucent clouds. Ann. Geophys. 33 (3), 363–366.

Gadsden, M., Schröder, W., 1989. Noctilucent Clouds. Springer-Verlag, Berlin.

Gadsden, M., Rothwell, P., Taylor, M.J., 1979. Detection of circularly polarised light from noctilucent clouds. Nature 278, 628–629.

Gumbel, J., Witt, G., 1998. In situ measurements of the vertical structure of a noctilucent cloud. Geophys. Res. Lett. 25 (4), 493–496.

Gumbel, J., Witt, G., 2001. Rocket-borne photometry of NLC particle populations. Adv. Space Res. 28 (7), 1053–1058.

Gumbel, J., Stegman, J., Murtagh, D.P., Witt, G., 2001. Scattering phase functions and particle sizes in noctilucent clouds. Geophys. Res. Lett. 28 (8), 1415–1418.

Gumbel, J., Siskind, D.E., Witt, G., Torkar, K.M., Friedrich, M., 2003. Influences of ice particles on the ion chemistry of the polar summer mesosphere. J. Geophys. Res. 108 (D8).

Heintzenberg, J., Witt, G., Kinnmark, I., 1964. Optical characteristics of noctilucent clouds: measurements and interpretation. In: Gadsden, M., Wraight, P.C. (Eds.), 6th Annual Meeting on Upper Atmosphere Studies by Optical Methods, Aberdeen, Scotland.

Hemenway, C.L., Witt, G., 1963. Particle sampling from noctilucent clouds. Nature 199, 269–270.

Hemenway, C.L., Fullam, E.T., Skrivanek, R.A., Soberman, R.K., Witt, G., 1964. Electron microscope studies of noctilucent cloud particles. Tellus 16 (1), 96–102.

Hervig, M., Thompson, R.E., McHugh, M., Gordley, L.L., Russell III, J.M., Summers, M.E., 2001. First confirmation that water ice is the primary components of polar mesospheric clouds. Geophys. Res. Lett. 28 (6), 971–974.

Heymsfield, A.J., 1986. Ice particles observed in a cirriform cloud at −83 °C and implications for polar stratospheric clouds. J. Atmos. Sci. 43, 851–855.

Hobbs, P.V., 1974. Ice Physics. Clarendon, Oxford.

Hunten, D.M., Turco, R.P., Toon, O.B., 1980. Smoke and dust particles of meteoric origin in the mesosphere and stratosphere. J. Atmos. Sci. 37, 1342–1357.

Jesse, O., 1886. Auffalende Abenderscheinungen am Himmel. Meteorol. Z. 2, 311–312.

Klostermeyer, J., 2002. Noctilucent clouds getting brighter. J. Geophys. Res. 107 (D14).

Kokhanovsky, A.A., 2001. Optics of Light Scattering Media. Springer-Praxis, Chichester.

Kokhanovsky, A.A., 2003. Polarization Optics of Random Media. Springer-Praxis, Berlin.

Kokhanovsky, A.A., 2004. Optical properties of terrestrial clouds. Earth-Sci. Rev. 64, 189–241.

Kondratyev, K.Ya., Buznikov, A.A., Vasilyev, O.B., Sevastyanov, V.I., 1971. On observations of noctilucent clouds from space. Dokl. Akad. Nauk Ukr. SSR 197 (5), 1066–1069.

Körner, U., Sonnemann, G.R., 2001. Global three-dimensional modeling of the water vapor concentration of the mesosphere–mesopause region and implications with respect to the noctilucent cloud region. J. Geophys. Res. 106 (D9), 9639–9651.

Leslie, R.C., 1885. Sky glows. Nature 32, 245.

Lübken, F.-J., Müllemann, A., 2003. First in situ temperature measurements in the summer mesosphere at very high latitudes (78°). J. Geophys. Res. 108 (D8), 8448.

Lübken, F.-J., Jarvis, M.J., Jones, G.O.L., 1999. First in situ temperature measurements at the Antarctic summer mesopause. Geophys. Res. Lett. 26, 3581–3584.

Ludlam, F.H., 1957. Noctilucent clouds. Tellus 9, 341–364.
Martie, J., Mauersberger, K., 1993. A survey and new measurements of ice vapor pressure at temperatures between 170 and 250 K. Geophys. Res. Lett. 20, 363–366.
Mayer, E., Hallbrucker, A., 1987. Cubic ice from liquid water. Nature 325, 601–602.
McHugh, M., Hervig, M., Magill, B., Thompson, R.E., Remsberg, E., Wrotny, J., Russell III, J., 2003. Improved mesospheric temperature, water vapor and polar mesospheric cloud extinctions from HALOE. Geophys. Res. Lett. 30 (8), 1440.
Mishchenko, M.I., 1991. Light scattering by nonspherical ice grains: an application to noctilucent cloud particles. Earth Moon, Planets 57, 203–211.
Purcell, E.M., Pennypacker, C.R., 1973. Scattering and absorption of light by nonspherical dielectric grains. Astron. J. 186, 705–714.
Rauser, P., Fechtig, H., 1972. Combined dust collection and detection experiment during noctilucent clouds display above Kiruna, Sweden. Space Res. 12, 391–402.
Roddy, J.W., 1986. The physics of noctilucent clouds formation. Collected Papers of International Workshop. Tallinn, pp. 33–58.
Rouleau, F., Martin, P.G., 1993. A new method to calculate the extinction properties of irregularly shaped particles. Astrophys. J. 414, 803–814.
Schmidlin, F.J., 1991. The inflatable sphere: a technique for the accurate measurement of middle atmosphere temperatures. J. Geophys. Res. 96, 22673–22682.
Shettle, E.P., Thomas, G.E., Olivero, J.J., Evans, W.F.J., Debrestian, D.J., Chardon, L., 2002. Three-satellite comparison of polar mesospheric clouds: evidence for long-term change. J. Geophys. Res. 107 (D12).
Stephens, G.L., 1994. Remote Sensing of Lower Atmosphere. Oxford University Press, New York.
Stevens, M.H., Conway, R.R., Englert, C.R., Summers, M.E., Grossmann, K.U., Gusev, O.A., 2001. PMCs and the water frost point in the Arctic summer mesosphere. Geophys. Res. Lett. 28, 4449–4452.
Svanberg, M., Ming, L., Markovic, N., Pettersson, J.B.C., 1998. Collision dynamics of large water clusters. J. Chem. Phys. 108 (14), 5888–5897.
Taylor, M.J., Gadsden, M., Lowe, R.P., Zalcik, M.S., Brausch, J., 2002. Mesospheric cloud observations at unusually low latitudes. J. Atmos. Sol.-Terr. Phys. 64, 991–999.
Thayer, J.P., Thomas, G.E., Lübken, F.-J., 2003. Foreword: layered phenomena in the mesopause region. J. Geophys. Res. 108 (D8), 8434.
Thomas, G.E., 1991. Mesospheric clouds and the physics of the mesopause region. Rev. Geophys. 29 (4), 553–575.
Thomas, G.E., McKay, C.P., 1985. On the mean particle size and water content of polar mesospheric clouds. Planet. Space Sci. 33 (10), 1209–1224.
Tozer, W.F., Beeson, D.E., 1974. Optical model of noctilucent clouds based on polarimetric measurements from two sounding rocket campaigns. J. Geophys. Res. 79 (36), 5607–5612.
Turco, R.P., Toon, O.B., Whitten, R.C., Keesee, R.G., Hollenbach, D., 1982. Noctilucent clouds: simulation studies of their genesis, properties and global influences. Planet. Space Sci. 30 (11), 1147–1181.
Van de Hulst, H.C., 1981. Light Scattering by Small Particles. Dover, New York.
Vasilyev, O.B., Rodionov, V.F., 1975. Optics of noctilucent clouds. Results of Studies on International Geophysical Projects, Physics of Mesosphere and Noctilucent Clouds. Meteorological Studies, vol. 22. Nauka, Moscow.
Von Cossart, G., Fiedler, J., von Zahn, U., 1999. Size distributions of NLC particles as determined from 3-colour observations of NLC by ground-based Lidar. Geophys. Res. Lett. 26, 1513–1516.
Von Savigny, C., Kokhanovsky, A.A., Bovensmann, H., Eichmann, K.-U., Kaiser, J., Noël, S., Rozanov, A.V., Skupin, J., Burrows, J.P., 2004. NLC detection and particle size determination: first results from SCIAMACHY on ENVISAT. Adv. Space Res. 34, 851–856.
Von Zahn, U., Berger, U., 2003. Persistent ice cloud in the midsummer upper mesosphere at high latitudes: three-dimensional modeling and cloud interactions with ambient water vapor. J. Geophys. Res. 108 (D8), 8451.
Warren, S.G., 1984. Optical constants of ice from the ultraviolet to the microwave. Appl. Opt. 23 (8), 1206–1225.
Willmann, Ch., Vasilyev, O.B., Avaste, O., 1973. Optical study of noctilucent clouds. Noctilucent Clouds. Optical Properties. Institute of Physics and Astrophysics of Estonian Academy of Sciences, Tallinn, pp. 61–75.
Witt, G., 1960. Polarization of light from noctilucent clouds. J. Geophys. Res. 65 (3), 925–933.
Witt, G., 1969. The nature of noctilucent clouds. Space Res. 9, 157–169.
Zakharova, N.T., Mishchenko, M.I., 2000. Scattering properties of needlelike and platelike ice spheroids with moderate aspect ratios. Appl. Opt. 39 (27), 5052–5057.